(Received 15 July 2025, Accepted 30 August 2025, Scheduled 11 September 2025)

An Efficient Center-Fed Dynamic Seawater Antenna

Xin Zhang, Lihua Li*, and Mingxuan Hu

Naval University of Engineering, Wuhan 430033, Hubei, China

ABSTRACT: In this paper, a high-efficiency, center-fed dynamic seawater monopole antenna is proposed. The antenna's radiation efficiency increases by raising the feed point position, adding a metal tube above the feed point, and reducing the inner diameter of the water pipe below the feed point. Concurrently, the effects of the feeding position, the length of the metal pipe, and the inner diameter of the water supply pipe on the current distribution are analyzed by theoretical modeling. FEKO electromagnetic simulation software is applied to simulate and analyze metal tubes with different lengths and water supply side pipes with different inner diameters. The simulation results indicate that the antenna attains optimal performance when being configured with a water supply pipe of 1 cm inner diameter and a 30 cm metal tube, achieving a maximum gain of 0.93 dBi and a peak radiation efficiency of 52%. Based on the simulation data, a simplified center-fed dynamic seawater antenna prototype is designed and fabricated. Experimental validation confirms that the seawater serves as the primary radiating element. The measured radiation characteristic curves exhibit consistent trends with the simulated results.

1. INTRODUCTION

In recent years, liquid-conductor antennas have emerged as a research hotspot in the antenna technology field due to the unique advantages of their fluidic structures, which enable reconfigurable frequency and radiation patterns [1, 2]. Among various conductive liquid materials, seawater has demonstrated significant potential in maritime platform applications such as Unmanned Surface Vehicles (USVs), owing to its easy accessibility and low cost [3, 4]. Based on the form of the radiating element, seawater antennas can be categorized into two fundamental types: static and dynamic. Both typically employ a cylindrical seawater as the radiator. Static seawater antennas utilize a sealed cylindrical container to store seawater in advance. In contrast, dynamic seawater antennas operate by pumping seawater into a drainage tube to form a seawater column in the air during operation; when the antenna is inactive, the pump is turned off, causing the seawater column to dissipate [5].

The efficiency of a seawater antenna is directly related to the radius of the seawater column. Within the skin depth, the radiation efficiency increases with the radius of the seawater column [6]. The height of the seawater column influences the antenna's resonant frequency and resonant points: as the height increases, the resonant frequency decreases while the number of resonant points increases [7]. Generally, once the radius and height of the seawater column are determined, the key factor governing antenna performance is the feeding structure. Static seawater antennas have a simple structure, typically employing a metal probe at the base for direct feeding into the liquid. In [6], by integrating a metallic disk at the antenna base, TM-mode excitation is enhanced, leading to an improved feed structure for higher radiation efficiency. Meanwhile, incorporating an insulating isolation layer at the base enables broadband seawater antenna design [8].

Compared to static seawater antennas, dynamic seawater antennas connect to a water pump via a pipe at the base. The presence of flowing seawater at the base makes feeding methods such as top-loaded metal disks unsuitable. Currently, the research on dynamic seawater antennas is relatively limited, including [5, 9–14]. The feeding methods for a seawater antenna can be divided into direct feeding and indirect feeding. The difference lies in whether the feeder makes direct contact with the seawater. Indirect feeding can be subdivided into two implementation approaches: magnetic loop coupling feeding and capacitive coupling feeding [5, 9]. However, magnetic loop coupling feeding suffers from low efficiency due to the high-loss ferrite materials, while capacitive coupling feeding exacerbates the challenge of resonant matching by increasing the system's capacitance, as the seawater antenna itself exhibits capacitive impedance [15]. Given these limitations, direct feeding has become the predominant choice.

For the feeding position, most dynamic seawater antennas are fed near the ground [10–12]. Base feeding results in current concentration near the ground, leading to strong electromagnetic coupling between the antenna and USV's surface. Variations in the ship's draft depth can alter the antenna's input impedance, increasing the demand for dynamic impedance matching. Additionally, feeding near the base causes part of the current to flow into the water below the surface, degrading radiation efficiency. Existing solutions involve adding a quarter-wavelength stub tube in series or parallel on the water supply side to short-circuit the current [13, 14]. However, this approach primarily suppresses the current on the water supply side. Besides, the quarter-wavelength stub tube becomes excessively long at high frequency (HF), hindering antenna miniaturization.

This paper presents a novel center-fed dynamic seawater antenna designed for operation in the high frequency (HF) band.

* Corresponding author: Lihua Li (0909031014@nue.edu.cn).

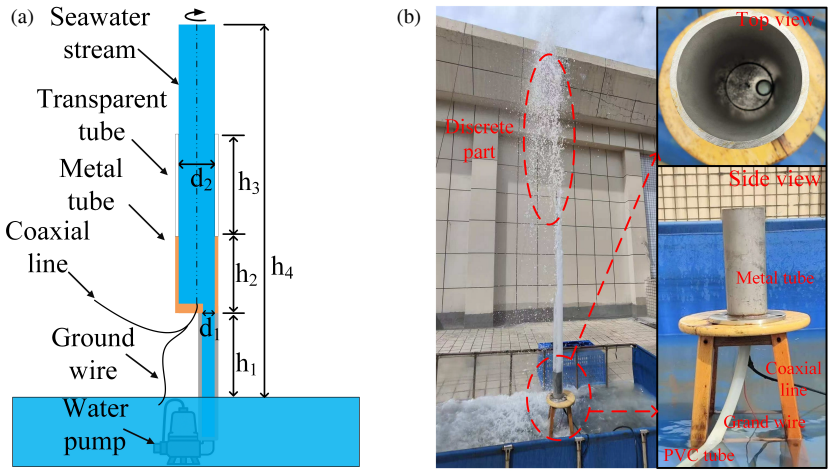

FIGURE 1. Proposed antenna: (a) Geometry of antenna, (b) photograph of antenna.

By elevating the feeding position, the current distribution is modified, reducing electromagnetic coupling between the antenna and mobile carrier's surface. Furthermore, the feeding structure is optimized: a metal tube is introduced above the feeding point, while a smaller-radius water pipe is used below the feeding point. This design enhances the current above the feeding point and effectively utilizes the current below it, thereby improving the antenna's radiation efficiency.

2. CENTER-FED SEAWATER ANTENNA STRUCTURE

Figure 1 illustrates the geometric structure of the center-fed seawater antenna and its physically fabricated prototype. In Figure 1(a), the antenna system primarily consists of four components: a Xinjie submersible water pump, a PVC pipe, a metal tube, and a feeding structure. The water pump is submerged in seawater, with its outlet connected to a PVC pipe. The PVC pipe with an inner diameter of d_1 extends above the water surface to a height of h_1, where it connects to a perforated metal tube. The metal tube comprises two components: a hollow cylindrical tube with inner diameter d_2 and height h_2, and a perforated disk with outer diameter d_1 tightly fitted at the base of the tube. The cylindrical tube enhances current above the feeding point, and the disk is to achieve TM mode excitation. Currently, limited by the water pump's power, we have added a transparent drainage tube with a length of h_3. It can be removed once the pump's power is sufficient to hold the water column. A coaxial cable is employed for the feeding structure, with its inner conductor passing through the disk's central aperture for direct contact, while the extended outer conductor connects to the seawater surface as ground. When the jet height exceeds h_4, the upper part of the water column gradually breaks apart and disperses, interrupting the current path. Therefore, the effective height h_4 of the seawater antenna should be defined as the maximum height at which the water column remains continuous, rather than the total jet height. For experimental support, a simple waterproofed insulating wooden stool ($\varepsilon_r \approx 5$) is employed. The dimensions of transparent tube and wooden stool are sufficiently small relative to operational wavelengths; therefore, their impact on antenna performance is negligible. Finally, the center-fed dynamic seawater antenna' parameters are summarized in Table 1.

TABLE 1. Details of the proposed antenna.

Parameters	h_1	h_2	h_3	h_4	d_1	d_2
Values (cm)	30	30	70	170	2	8

3. ANTENNA ANALYSIS

Figure 2 illustrates the schematic diagram of a dynamic seawater antenna with different feed positions. Due to the presence of the water pump, part of the current inevitably flows through the water pipe toward the area below the sea surface, resulting in an asymmetric dipole antenna structure. When the feed point is located near the ground with the lower section of the antenna immersed in seawater, the severe skin effect and substantial energy loss occurring during electromagnetic wave propagation in seawater lead to a drastic reduction in radiation efficiency for currents below the feed point. Consequently, the contribution of these currents to effective radiation becomes negligible.

Additionally, adopting a bottom-fed configuration causes the current to concentrate in the lower region of the antenna. When the seawater antenna is installed on a mobile unmanned vessel, strong electromagnetic coupling occurs between the antenna and ship's surface. Since the vessel's draft depth varies with its navigation state, the surface structure changes accordingly, leading to fluctuations in the antenna's input impedance and ultimately causing the preset impedance matching device to fail.

As shown in Figure 2(b), appropriately raising the feed position can effectively utilize the current distribution below the feed point, thereby improving the overall radiation efficiency of the antenna. Ideally, the feed point should be located at the top of the seawater antenna to achieve optimal performance. However, for a dynamic seawater antenna, the highest feasible feed point is defined by the water outlet (at height $h_1 + h_2$), as the antenna itself is a jet of seawater. From a theoretical perspec-

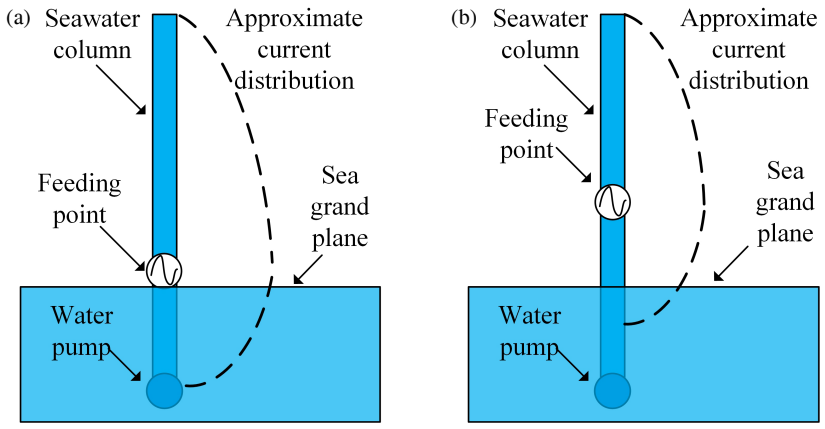

FIGURE 2. Dynamic seawater antennas with different feed positions: (a) bottom feeding, (b) center feeding.

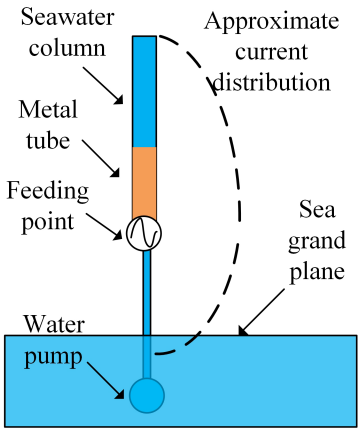

FIGURE 3. Proposed antenna model.

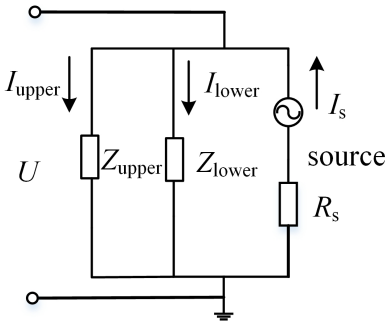

FIGURE 4. Analogous circuit model.

tive, to fully leverage the performance advantages of seawater antennas, the ideal water outlet height should be zero (i.e., the water column sprays directly from the ground). However, this design would impose extremely high-power demands on the pump system. Engineering practice has shown that appropriately increasing the water outlet height can effectively reduce the power of the pump. Based on comprehensive analysis, it is recommended that the ratio of the water outlet height to the total antenna height (h_1+h_2/h_3) should not exceed 40% in our paper. Given the center-fed dynamic seawater antenna in this study, it is recommended that the feed position of a dynamic seawater antenna is at the midpoint of the water outlet height, i.e., $h_1 = h_2$.

Figure 3 illustrates the novel center-fed seawater antenna. As shown in Figure 3, since the feed height of the dynamic seawater antenna should not be excessively high, this study introduces a metal tube above the feed point and employs a small-radius water pipe below the feed point after increasing the feed height of the seawater antenna. Figure 4 illustrates the equivalent circuit diagram of dynamic seawater antenna. As depicted in Figure 4, the antenna is divided into an upper section and a lower section at the feed point. Z_{upper} and Z_{lower} represent the impedances of the upper and lower sections of the seawater antenna, respectively. I_{upper} and I_{lower} denote the currents in the upper and lower sections of the feed point, respectively. I_s and R_s correspond to the source current and internal resistance of the power supply, respectively. Since the primary radiating element of the antenna is the part above the seawater surface, according to the definition of the effective height of an antenna, the effective height of the upper section of the antenna at the feed point can be expressed as [16]:

$$h_e = \frac{1}{I_{upper}(h_1)} \int_{h_1}^{h_3} I_{upper}(z)dz \tag{1}$$

A smaller upper-section current I_{upper} would reduce the effective height of the antenna, adversely affecting its radiation efficiency. To increase the antenna's effective height, it is necessary to minimize the downward current I_{lower} while maximizing the upward current I_{upper}. According to Kirchhoff's Current Law (KCL), I_{upper} and I_{lower} satisfy the following relationship:

$$I_s = I_{upper} + I_{lower} \tag{2}$$

$$I_{upper} = \frac{U}{Z_{upper}}, \quad I_{lower} = \frac{U}{Z_{lower}}. \tag{3}$$

Therefore, the improvement of the antenna's effective height can be achieved by impedance adjustment, making the downward impedance Z_{lower} as large as possible while minimizing the upward impedance Z_{upper}. According to [17], when the seawater antenna radius is smaller than the skin depth, its surface

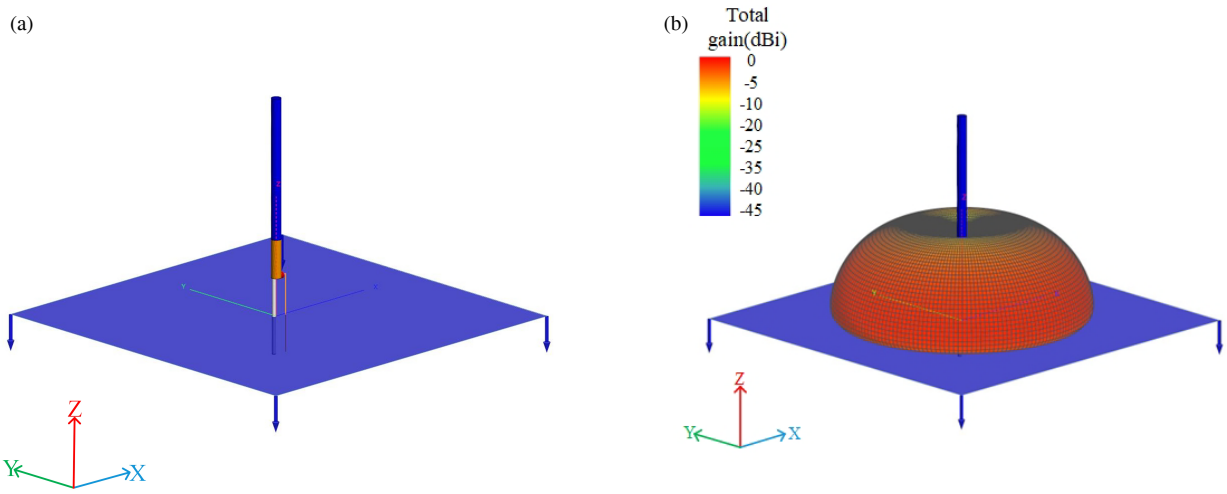

FIGURE 5. Simulation of the seawater antenna. (a) Basic model, (b) 3D radiation pattern.

resistance is given by:

$$Z = \frac{1}{r\sigma} \tag{4}$$

where r represents the radius of the seawater column, and σ denotes the conductivity of seawater. That is, within the skin depth, the surface resistance of seawater increases as the radius decreases. Therefore, for the lower-section impedance Z_{lower}, it can be increased by reducing the radius of the lower seawater column. Under ideal conditions, if the lower-section radius is reduced to zero, a static monopole antenna can be formed, completely isolating the water-supply currents. To accommodate the implementation of a dynamic seawater antenna, the radius of the water pipe can be appropriately reduced. When the seawater antenna radius exceeds the skin depth, its surface resistance is given by:

$$Z = \frac{1+j}{d_s\sigma} \tag{5}$$

where d_s denotes the skin depth of seawater. Given a seawater conductivity of 4 S/m, the corresponding skin depth in the 30–100 MHz frequency range is 4.5–2.5 cm. When the seawater column radius exceeds the skin depth, its surface resistance remains essentially constant. Therefore, for the upper-section impedance Z_{upper}, it can be reduced by increasing the radius of the upper seawater column to at least the skin depth.

Additionally, this study introduces a metallic section at the upper portion of the seawater antenna, forming a hybrid seawater-metal antenna structure. Due to the extremely high conductivity of the metal, current primarily concentrates on its surface, thereby reducing Z_{upper}. However, an excessively long metal feed tube would cause current to predominantly flow along the conductor, shifting the primary radiating element to the metal section and diminishing the significance of the seawater antenna. Thus, the length of the metal tube should be optimized to balance performance. Considering the relationship between the feed point height and water outlet height, the maximum length of the metal tube is limited to 30 cm in this paper.

4. SIMULATION ANALYSIS

This study employs FEKO electromagnetic simulation software to conduct numerical analysis of the dynamic seawater antenna. During the modeling process, two key aspects are addressed. First, the continuous seawater jet ejected into the air gradually breaks up into discrete droplets over time due to Rayleigh-Plateau instability [18, 19]. Considering the attenuation of conduction current in the terminal droplets, the effective height of the seawater column is set at 1.7 m — the portion below this height is treated as a complete cylinder, while the discrete droplets above 1.7 m are neglected. Second, for the underwater structure, the seawater column below the sea surface should adopt an insulated PVC pipe encapsulated structure model. This model must ensure complete isolation between the main seawater column and external seawater, with only the pipe's end cross-section simulating contact with the seawater. Additionally, since the length of the supporting wooden stool is much smaller than the operating wavelength, its influence on the radiation characteristics is disregarded. Based on the antenna parameters listed in Table 1, the final simulation model is presented in Figure 5(a). As shown in Figure 5(b), influenced by the reflection effect of the sea surface, the antenna exhibits monopole-like characteristics, demonstrating omnidirectional radiation patterns below the horizontal plane. To evaluate the influence of the length of the metal tube h_2 on antenna performance, simulations are conducted under controlled variables to analyze the effects on the antenna's radiation characteristics.

Figure 6 illustrates radiation characteristics of the dynamic seawater antenna with different lengths of the metal tube. As shown in Figure 6(a), the resonant frequency is 30 MHz, and increasing the length of the metal tube does not alter the resonant frequency or bandwidth. Figure 6(b) reveals that as the length of the metal tube increases, the radiation efficiency also improves. At the resonant frequency (30 MHz), the antenna with a 30 cm metal tube achieves a radiation efficiency of approximately 37%, representing a 5% improvement compared to a 1 cm metal tube. Figures 6(c) and (d) depict the radiation patterns at 30 MHz. As the length of the metal tube increases,

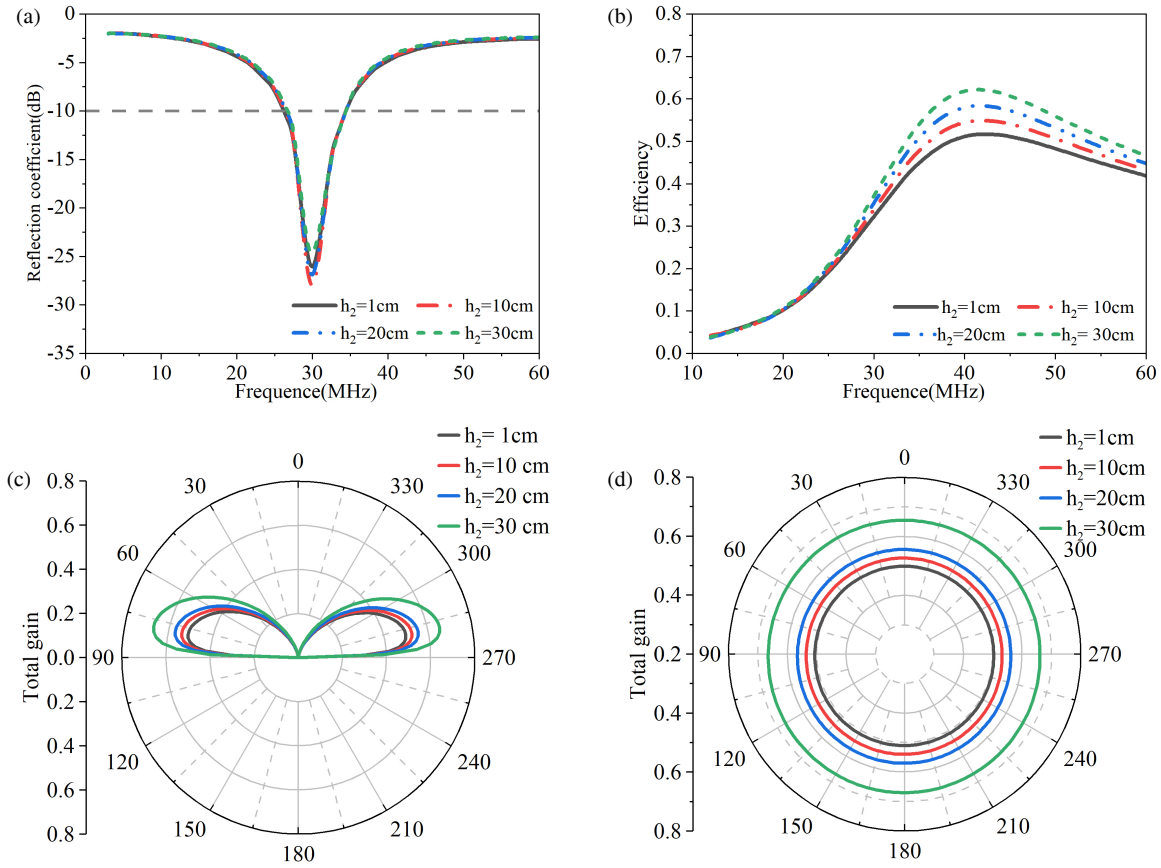

FIGURE 6. Simulated antenna radiation characteristics with different metal tube lengths: (a) reflection coefficient, (b) radiation efficiency, (c) E-plane radiation pattern at 30 MHz, and (d) H-plane radiation pattern at 30 MHz.

the total gain shows an upward trend, with the maximum gain approximately 0.65 dBi achieved at a 30 cm length.

Similarly, to study the influence of the inner diameter of the PVC pipe d_1 on antenna performance, under fixed structural parameters, simulations are performed to analyze the effects on the antenna's radiation characteristics. Based on the previous simulation results, the length of metal tube is set to 30 cm. Figure 7 illustrates the antenna's radiation characteristics with different inner diameters of the PVC pipe. As can be seen in Figure 7(a), the resonant frequency is around 30 MHz. Reducing the inner diameter of the PVC pipe slightly lowers the resonant frequency. A PVC pipe with an inner diameter of 4 cm corresponds to a resonant frequency approximately 33 MHz, while a 1 cm inner diameter results in a resonant frequency of 27 MHz. As the radius decreases, the -10 dB bandwidth also narrows. In Figure 7(b), as the inner diameter of the PVC pipe decreases, the radiation efficiency increases. At 30 MHz, compared to a 4 cm inner diameter PVC pipe, a 1 cm inner diameter pipe achieves a radiation efficiency of 52%, while the 4 cm pipe yields 25%, representing a 27% improvement. Figures 7(c) and (d) show the radiation patterns at 30 MHz. As the inner diameter of the PVC pipe decreases, the total gain exhibits an upward trend, with the maximum gain approximately 0.93 dBi achieved at a 1 cm inner diameter. Finally, the simulation results agree with the analysis in Section 3.

5. EXPERIMENTS ANALYSIS

The experiment is conducted in a seawater pool, with the pool measuring 5 meters in length and 3 meters in width. The conductivity of the seawater in the pool is 5 S/m. Due to the limitations imposed by the pump head and power constraints in the experimental setup, employing PVC pipes with excessively small inner diameters would result in excessive hydraulic pressure, exceeding the pump's rated power capacity. Consequently, the inner diameter of fabricated PVC pipes is 2 cm. Due to the dynamic seawater antenna's unique characteristics, it is challenging to measure its radiation pattern and radiation efficiency. For the measurement of radiation characteristics of dynamic seawater antennas, this paper employs the comparative method from [12], which indirectly evaluates antenna performance through Signal-to-Noise Ratio (SNR) measurements. To assess antenna radiation properties, transmission experiment was conducted using a signal generator on a seawater pool platform, while the G39 signal receiver performed reception measurements at a distance of 200 meters from the pool. Figure 8 illustrates the testing scenario of the center-fed seawater antenna.

Prior to the experiments, to verify that seawater is the primary radiating element of the dynamic seawater antenna, Vector Network Analyzer (VNA) is employed to measure the reflection coefficients in both spraying and non-spraying states. Figure 9 presents the reflection coefficients experimental re-

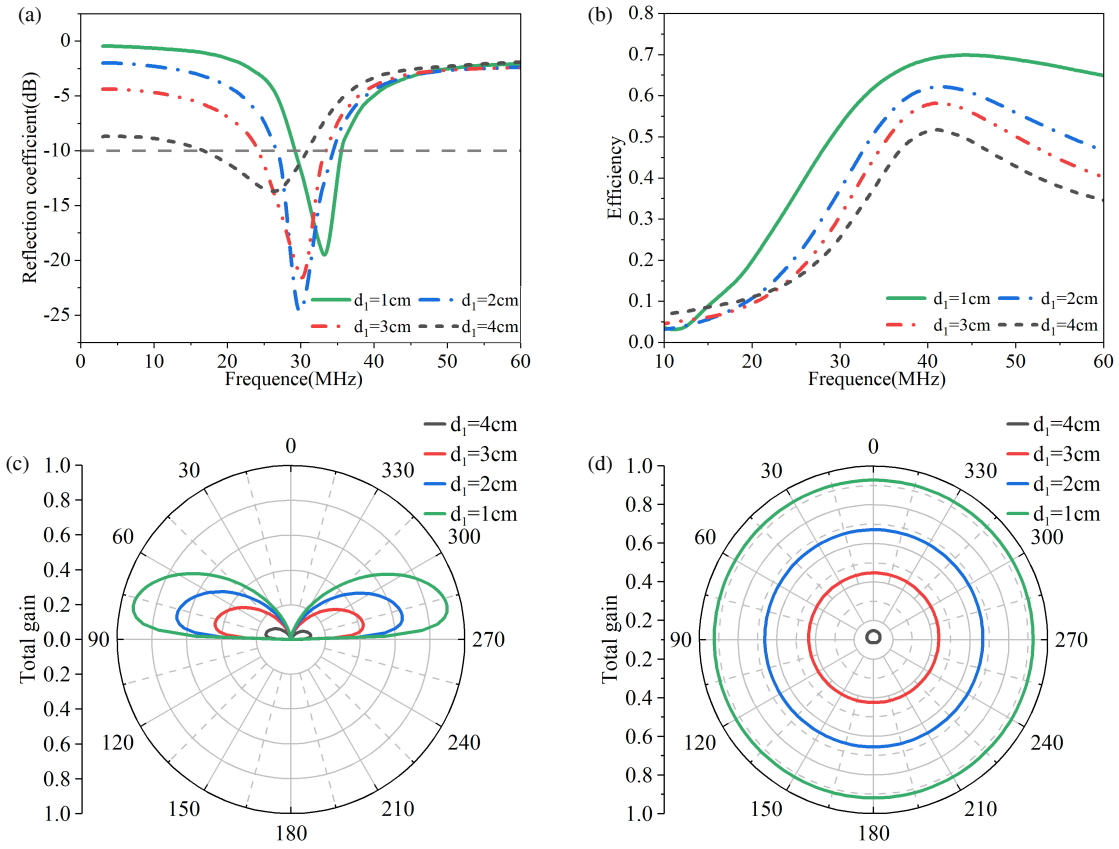

FIGURE 7. Simulated antenna radiation characteristics with different different PVC pipe inner diameters: (a) reflection coefficient, (b) radiation efficiency, (c) E-plane radiation pattern at 30 MHz, and (d) H-plane radiation pattern at 30 MHz.

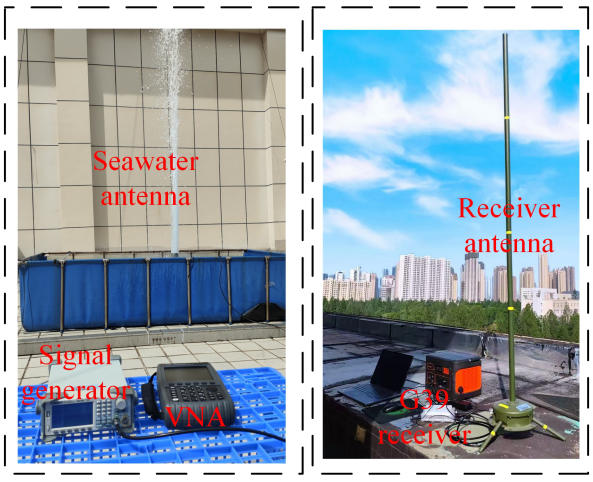

FIGURE 8. Antenna test environment.

sults of the center-fed dynamic seawater antenna. As depicted in Figure 9, within the 10–60 MHz frequency range, no significant resonance points are observed in the non-spraying state, and the reflection coefficient remained above -5 dB, indicating severe impedance mismatch where most incident energy is reflected. In contrast, during the spraying state, a distinct resonance point appeared at 28 MHz, closely aligning with the simulated resonance frequency. The reflection coefficient is below -10 dB in the 15–33 MHz range. This comparative result confirms that seawater is the primary radiating element of the dynamic seawater antenna.

For signal transmission, a sinusoidal signal with an amplitude of 5 V is used. Based on VNA measurements, the transmission frequency range is selected as 10–60 MHz. To mitigate interference from coexisting signals at specific frequencies (e.g., 10 MHz), the transmission frequencies are configured with a 3 MHz step size, spanning from 12.5 MHz to 57.5 MHz, yielding a total of 16 discrete frequency points. During signal reception, the background noise level is first measured at each frequency point, followed by transmission using the seawater antenna. The received signal level is then measured, and the SNR is derived from the difference between the signal level and background noise. It is known that the variation in the received signal's SNR is positively correlated with the realized gain of the seawater antenna. Figure 10 shows measured SNR and simulated realized gain. As shown in Figure 10, the SNR first increases and then decreases with frequency, reaching its peak value of 43 dB at 33 MHz. This trend aligns with the simulated realized gain curve, further verifying the consistency between the antenna's radiation characteristics and simulation results.

At 28 MHz, the measured realized gain is estimated about -4 dBi (linear gain ≈ 0.4), lower than the simulated value of 0.5. In practical measurements, the antenna gain is lower than the simulation results primarily due to two reasons: Firstly, the

TABLE 2. Comparison with pervious literature.

References	height (m)	Frequence band	Resonant frequency (MHz)	Gain (dBi)	Impedance Bandwidth (%)
[9]	N.A.	VHF	110	−0.2	27
[10]	0.1	VHF	540	N.A.	14
[11]	1.3	VHF	215	N.A.	0
[12]	1	VHF	56.5	2.5	19.8
this	1.7	HF/VHF	28	−4	75

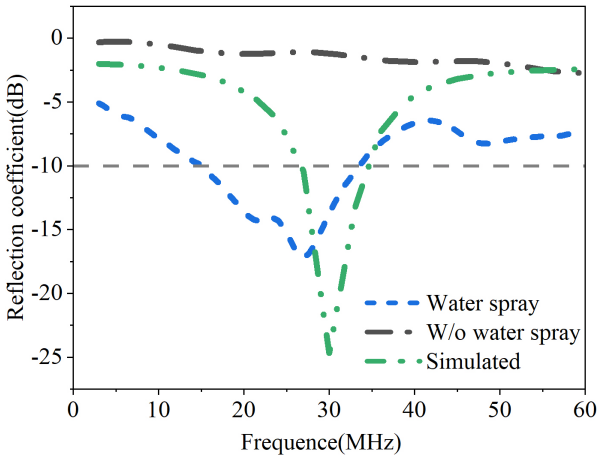

FIGURE 9. Simulated and measured S_{11}.

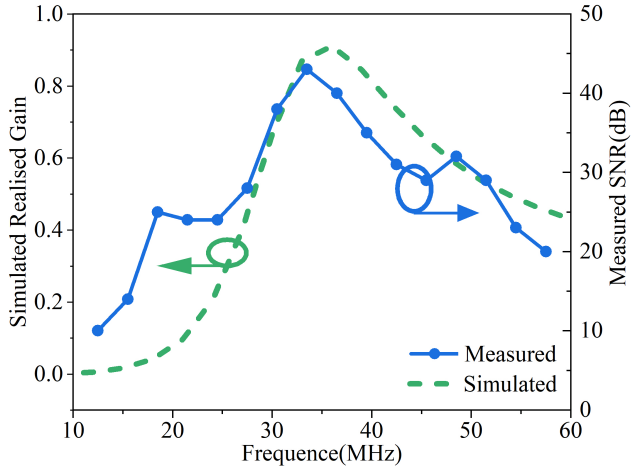

FIGURE 10. Measured SNR and simulated relised gain.

simulation model assumes an infinite sea surface as the ground with high conductivity (approximately 4 S/m), which provides an ideal reflective surface and a ground current return path. However, the experimental environment consists of two types of ground surfaces: a limited-size seawater pool and the surrounding dry floor. The dry ground has extremely low conductivity (typically only 0.005 S/m), which is significantly different from that of seawater. This nonuniform ground introduces additional losses, leading to a reduction in actual gain. Secondly, due to limitations in pump power and flow rate, the cross-section of the practically formed water jet does not fully reach the inner diameter size of the metal tube, resulting in a reduced effective conductive cross-sectional area. This increases the ohmic loss in the seawater jet, thereby reducing the realized gain.

Table 2 presents a comparison among existing dynamic seawater antennas. As can be seen, the proposed seawater antenna exhibits significantly wider impedance bandwidth than existing counterparts. Operating in the HF band, it demonstrates strong potential for medium to long range maritime communication applications. However, due to its relatively small electrical size and experimental constraints, the gain of our antenna remains lower than other seawater antennas.

6. CONCLUSION

A high-efficiency center-fed structure of dynamic seawater antenna is proposed in this paper. The length of the metal tube and the inner diameter of the PVC pipe are analyzed in detail by FEKO software simulation. In order to achieve efficient seawater antenna, the length of the metal tube should be as long as possible under the premise that seawater is the main radiator. Under the premise of the realization of the dynamic seawater antenna, the inner diameter of the water supply side pipe should be small. The actual effect of the center-fed seawater antenna is verified by the seawater pool platform. Due to the limitation of experimental constraints, the realized gain of seawater antenna could be reduced. In the future study, actual sea experiments will be carried out.

ACKNOWLEDGEMENT

This work was supported in part by the National Natural Science Foundation of China (42174045) and the Self-Developed Scientific Research Project of Naval University of Engineering (2025236).

REFERENCES

[1] Dey, A., R. Guldiken, and G. Mumcu, "Microfluidically reconfigured wideband frequency-tunable liquid-metal monopole antenna," *IEEE Transactions on Antennas and Propagation*, Vol. 64, No. 6, 2572–2576, Jun. 2016.

[2] Wang, M., Z. Zhang, and A. Chen, "Ultrawideband pattern reconfigurable planar monopole antenna based on liquid metal," *IEEE Antennas and Wireless Propagation Letters*, Vol. 23, No. 11, 3734–3738, Nov. 2024.

[3] Huang, Y., L. Xing, C. Song, S. Wang, and F. Elhouni, "Liquid antennas: Past, present and future," *IEEE Open Journal of Antennas and Propagation*, Vol. 2, 473–487, Mar. 2021.

[4] Sayem, A. S. M., A. Lalbakhsh, K. P. Esselle, G. Moloudian, J. L. Buckley, and R. B. V. B. Simorangkir, "Advancements, challenges, and prospects of water-filled antennas," *IEEE Access*, Vol. 11, 8301–8323, Jan. 2023.

[5] SPAWAR, "Sea water antenna system," SSC Pacific, San Diego, CA, Apr. 2011 [Online]. Available: http://www.public.navy.mil/spawar/Pacific/TechTransfer/Prod-uctsServices/Pages/SeaWaterAntennaSystem.aspx and https://www.youtube.com/watch?v=9tIZUhu21sQ, Apr. 2011.

[6] Hua, C., Z. Shen, and J. Lu, "High-efficiency sea-water monopole antenna for maritime wireless communications," *IEEE Transactions on Antennas and Propagation*, Vol. 62, No. 12, 5968–5973, Dec. 2014.

[7] Xing, L., Y. Huang, Y. Shen, S. A. Ja'afreh, Q. Xu, and R. Alrawashdeh, "Further investigation on water antennas," *IET Microwaves, Antennas & Propagation*, Vol. 9, No. 8, 735–741, Jun. 2015.

[8] Xing, L., Y. Huang, S. S. Alja'afreh, and S. J. Boyes, "A monopole water antenna," in *2012 Loughborough Antennas & Propagation Conference (LAPC)*, 1–4, Loughborough, UK, 2012.

[9] Hua, C. and Z. Shen, "Sea-water half-loop antenna for maritime wireless communications," in *2015 IEEE 4th Asia-Pacific Conference on Antennas and Propagation (APCAP)*, 231–232, Bali, Indonesia, 2015.

[10] Akimoto, S., T. Yanagi, T. Fukasawa, and H. Miyashita, "Demonstration of a highly efficient seawater antenna," in *2016 IEEE-APS Topical Conference on Antennas and Propagation in Wireless Communications (APWC)*, 55–58, Cairns, QLD, Australia, 2016.

[11] Li, L., S. Feng, and M. Xiu, "Inductive reactance isolated dynamic seawater monopole antenna of high efficiency," *Applied Computational Electromagnetics Society Journal (ACES)*, Vol. 38, No. 12, 952–957, Dec. 2023.

[12] Hua, C. and Z. Shen, "Shunt-excited sea-water monopole antenna of high efficiency," *IEEE Transactions on Antennas and Propagation*, Vol. 63, No. 11, 5185–5190, Nov. 2015.

[13] Lv, Z., X. An, Y. Wang, X. Shan, and Q. Lv, "A conductive liquid antenna," China Patent 110994149A, 2019.

[14] Mitsubishi Electric Corporation, "Antenna device," China Patent 105940555B, 2017.

[15] Yang, Z., "Preliminary study on seawater antenna," *Ship Electronic Engineering*, Vol. 31, No. 12, 101–103, 2011.

[16] Balanis, C. A., *Antenna Theory*, Wiley, 1997.

[17] Qian, Y., "Wideband high efficiency hybrid liquid antennas," Ph.D. dissertation, South China University of Technology, Guangzhou, China, 2017.

[18] Frohn, A. and N. Roth, *Dynamics of Droplets*, Springer Science & Business Media, 2000.

[19] Zhang, B., P. Cheng, Q. L. Li, H. Y. Chen, and C. Y. Li, "Breakup process of liquid jet in gas film," *Acta Physica Sinica*, Vol. 70, No. 5, 054702, 2021.